https://www.aimspress.com/journal/mine

Mathematics in Engineering, 7(4): 481–504.
DOI:10.3934/mine.2025020
Received: 04 February 2025
Revised: 16 May 2025
Accepted: 25 July 2025
Published: 04 August 2025

Research article

A double free boundary problem on microbially induced corrosion in wastewater concrete

Antonella Capuozzo, Alberto Tenore*, Fabiana Russo and Luigi Frunzo

Department of Mathematics and Applications "Renato Caccioppoli", University of Naples Federico II, Via Cintia, Monte S. Angelo, Naples, 80126, Italy

* **Correspondence:** Email: alberto.tenore@unina.it.

Abstract: Microbially influenced corrosion (MIC) refers to any corrosion process caused or fostered by microbial activity, and represents a global concern, impacting infrastructure, economies, and the environment worldwide. MIC affects a wide range of materials and is particularly common in wastewater concrete pipes, where it is associated with the proliferation of biofilm colonies of sulfur-oxidizing bacteria (SOBs). SOBs oxidize hydrogen sulfide produced within wastewater effluents and generate corrosive sulfuric acid that triggers the degradation of concrete. We propose here a one-dimensional, two-layer diffusion model with double free boundaries to investigate the proliferation of SOB biofilms and the related corrosion process in wastewater concrete pipes. The domain is composed of two free boundary regions: a monospecies SOB biofilm in contact with the sewer atmosphere, which grows towards the interior cavity of the pipe, sitting on a gypsum layer formed from corrosion, that penetrates the concrete pipe. Diffusion-reaction equations govern the transport and metabolic production or consumption of hydrogen sulfide, oxygen, and sulfuric acid within the biofilm layer. The biofilm free boundary tracks the growth of the microbial community, regulated by metabolic activity of SOBs and detachment phenomena. The corrosion process is incorporated in the model through a Stefan-type condition, which drives the advancement of the gypsum free boundary into the concrete pipe, governed by microbial production of sulfuric acid. Numerical simulations are carried out to investigate the model behavior, encompassing the development and progression of the biofilm as well as the corrosion advancement, with the aim of elucidating the influence of key factors such as hydrogen sulfide level in the sewer, calcium carbonate concentration in concrete, detachment phenomena, and acid diffusivity in the gypsum layer. Interestingly, the model suggests that, under specific conditions, biofilms may impose limitations on sulfuric acid diffusion and act as a partial protective barrier for the underlying concrete.

Keywords: microbially induced corrosion; concrete corrosion; biofilms; free boundary problems; numerical simulations

1. Introduction

Microbially influenced corrosion (MIC), also known as biocorrosion, refers to any corrosion process induced or fostered by microbial activity. It affects a wide range of materials and environments, depending on microbial taxonomy and environmental conditions [21, 43]. MIC is recognized as a leading cause of corrosion-related failures, and estimated to contribute to approximately 20%–50% of the global annual cost of corrosion, amounting to hundreds of billions of dollars [43, 56].

Concrete, the most commonly used building material worldwide, is notably susceptible to biocorrosion [37]. This process is associated with metabolic activity of specific microorganisms, namely Sulfur-Oxidizing Bacteria (SOBs). They oxidize hydrogen sulfide H_2S on the moist concrete surface to sulfuric acid SO_4^{2-}, a corrosive agent which attacks concrete components, thereby compromising the integrity of concrete structures [52]. SOB microorganisms mostly live in biofilms, microbial communities that adhere to a surface and are embedded within a self-produced extracellular matrix of polymeric substances, which provides protection and support to the microbial community [3].

The proliferation of SOB biofilms poses a substantial risk of concrete corrosion, especially in sewer systems. The interior surfaces of concrete sewer pipes, particularly those above the waterline, present favorable conditions for SOBs growth. These conditions include high moisture levels and large presence of essential compounds for SOB metabolism, such as oxygen and hydrogen sulfide, with the latter typically produced within wastewater effluents [32].

Within this framework, numerous mathematical models have been proposed in recent years to investigate biofilm dynamics across diverse environments [15, 47, 48], including studies specifically targeting concrete wastewater pipes [6, 7, 55]. These efforts aim to understand, predict, and manage biofilm processes, ultimately contributing to more sustainable and resilient infrastructure systems. Specifically, Bohm et al. [6, 7] formulated a one-dimensional, one-phase moving boundary problem to study the biocorrosion process in sewer pipes, introducing a Stefan-type problem to capture the effects of calcite transformation into gypsum. Gypsum serves here as a layer of interconnected pores and fissures populated by cultures of sulfide-oxidizing microorganisms. In 2014, Yuan et al. [54] proposed a reactive transport model to describe the neutralization process of concrete by H_2S gas, including factors such as gas absorption, dissolution of portlandite, decalcification of calcium silicate hydrates, and precipitation of calcium sulfide. Later, the same authors incorporated in their model the production of sulfuric acid by SOBs, and the subsequent chemical reaction with cement hydration products, leading to corrosion [55]. However, in this model the surface neutralization and biodeterioration processes are simulated separately rather than continuously. Additional modeling studies focused on specific phases of the biocorrosion process. Vollertsen et al. [49] conducted experimental quantification of hydrogen sulfide absorption and oxidation on corroding concrete surfaces, proposing a kinetic expression to model the gathered data. Jensen et al. [18] modeled the hydrogen sulfide oxidation pathway in a matrix of corroded concrete and the growth of SOBs through a system of ordinary differential equations (ODEs), without considering the spatial evolution of the phenomenon. Nikolopoulos [31] proposed macroscopic models to study the concrete corrosion due to sulfation, including the formation of a mushy region. These models were derived through multiple-scale methods applied to the microscopic Stefan-type problem introduced in Bohm et al. [6]. Fedosov and Loginova [12] tracked the concentration of the target component of free calcium hydroxide in a one-dimensional concrete-biofilm system, through a parabolic partial differential equation accounting for diffusive mass transport

and microbial proliferation, quantified as a change in density. However, this work models microbial growth as a generical stochastic process, without specific reference to the metabolic activities of SOBs or the chemical compounds involved in the process. Additionally, they assume a fixed concrete layer domain without considering the effect of corrosion on its thickness. Finally, Clarelli et al. [10] and Bretti et al. [8] propose some free boundary problems that describe degradation processes in concrete, accounting for both swelling and shrinkage of the material.

Notably, to the best of our knowledge, there are currently no literature works that model the spatial growth of an SOB biofilm and how it affects the corrosion process in concrete. In the light of this, we propose here a one-dimensional, two-phase diffusion model with double free boundaries aimed at describing the biofilm dynamics and the spatial evolution of the corrosion front. The model is formulated in a continuum two-layer domain: A biofilm layer in contact with the sewer atmosphere, sitting on a gypsum layer, resulting from corrosion, that penetrates the concrete pipe. The biofilm domain is represented as a growing monospecies colony of SOBs, where hydrogen sulfide H_2S, oxygen O_2 and sulfuric acid SO_4^{2-} diffuse and are metabolically produced or consumed. The biofilm boundary is regulated by SOB metabolic growth processes and detachment phenomena. The Stefan-type problem introduced by Bohm et al. [6] is incorporated to model the corrosion phenomenon. Sulfuric acid, produced within the biofilm, permeates the gypsum layer and reacts upon contact with the uncorroded concrete, thereby causing the corrosion front to advance.

A numerical investigation is conducted to elucidate key aspects of the model, encompassing the formation and evolution of the biofilm as well as the advancement of corrosion. Original numerical simulations describe the effects of significant model parameters on the process. Specifically, we explore: The impact of hydrogen sulfide level in the pipeline, calcium carbonate concentration in the concrete, detachment phenomena, diffusivity of acid in the gypsum layer, and the rate of acid leaks at the sewer atmosphere-biofilm interface. The results shed light on how these parameters influence biofilm dynamics, corrosion progression, and concentration profiles of key substrates within the system. Moreover, they propose an interesting conclusion: Depending on their thickness, biofilms — beyond their traditionally assumed role as contributors to corrosion — may significantly restrict the diffusion of sulfuric acid toward the concrete surface, thereby acting as a protective barrier that mitigates the rate of corrosion.

The work is organized as follows: Section 2 introduces the problem of biocorrosion of concrete, including important biological, chemical and physical aspects; Section 3 describes the mathematical model, including assumptions, variables, equations, and initial and boundary conditions; Section 4 presents and discusses the numerical results; lastly, Section 5 outlines conclusions and future objectives.

2. Biocorrosion in concrete wastewater pipes

Microbially influenced corrosion was initially documented in the literature by Olmstead and Hamlin [33] while studying the corrosion of sewage pipelines in concrete. Later, Parker [34] recognized the pivotal role of SOBs in concrete corrosion, able to oxidize H_2S and produce corrosive metabolites. SOBs typically live in biofilms, aggregates of microbial cells attached to a solid surface and incorporated into a matrix of self-produced extrapolymeric substance, which provides stability and resistance to the aggregate [13, 14]. The biofilm lifecycle comprises different phases. After an

initial adhesion stage, microcolonies evolve into a mature biofilm, constituting a complex cellular structure characterized by water channels and pores. These porous architecture plays a crucial role in facilitating the diffusion of nutrients [41]. Once the biofilm becomes mature, individual cells or clusters may detach from the surface, due to external stressors like erosive shear stresses, as well as internal factors such as microbial death [24]. Importantly, microbial cells living in biofilms have the ability to cooperate, if necessary, in metabolic, reproductive, and infectious processes and may affect the physical, chemical, and electrochemical properties of the environment where they proliferate [5].

The walls of wastewater pipes above the waterline provide an ideal environment for SOB biofilm formation, i.e., high concentrations of hydrogen sulfide, moisture, and oxygen [32]. The difference in temperature between sewer atmosphere and sewage results in elevated relative humidity, fostering moisture condensation on sewer walls exposed to air [53]. This condensation establishes the favorable environment for biochemical reactions and promotes microbial proliferation [37]. H_2S is generated as a by-product from anaerobic degradation of sulfur compounds present in wastewater by sulfate-reducing bacteria (SRB) [29, 38, 53]. Due to its volatility, H_2S is released from wastewater and accumulates on the concrete surfaces exposed to air, where it reacts with CO_2 to neutralize the exposed concrete section. This process establishes a favorable environment for SOBs to proliferate, thus initiating the biofilm formation and the associated biocorrosion process [37].

As SOBs colonize concrete surfaces and develop biofilms, they metabolize hydrogen sulfide and oxygen, and produce sulfuric acid, according to the following biochemical reaction:

$$H_2S + 2\,O_2 \longrightarrow H_2SO_4 \longleftrightarrow 2\,H^+ + SO_4^{2-} \tag{2.1}$$

The sulfuric acid produced reacts with the constituents of the concrete matrix, causing progressive material deterioration and leading to the formation of gypsum ($CaSO_4 \cdot 2H_2O$). Building on previous studies [6, 7], we consider here a mature concrete – mainly composed of calcium carbonate ($CaCO_3$) [25] – which is of particular interest due to its increased susceptibility to severe degradation in sewage environments [22]. For this type of material, the main chemical process driving corrosion is described by the following reaction:

$$2\,H_2O + H^+ + SO_4^{2-} + CaCO_3 \longrightarrow CaSO_4 \cdot 2\,H_2O + HCO_3^- \tag{2.2}$$

The presence of gypsum compromises infrastructure reliability by weakening the structural integrity of pipes, increasing vulnerability to environmental stressors, and reducing overall durability [52].

3. Mathematical model

We propose a double free boundary problem to model the biofilm proliferation and the related biocorrosion process in concrete wastewater pipes. The biofilm-gypsum system is formulated as a one-dimensional two-layer domain (depicted in Figure 1). The biofilm-gypsum interface is assumed to be fixed, and located at $x = 0$. The biofilm layer is defined for $-L_1(t) \le x \le 0$, where $L_1(t)$ denotes the biofilm thickness, and the gypsum layer for $0 < x \le L_2(t)$, where $L_2(t)$ denotes the gypsum layer thickness. Both the biofilm and gypsum regions are assumed to grow perpendicularly to the interface, in the x-direction. The biofilm is modeled as a single species domain composed of SOBs, with a constant microbial density X_{SOB}. The biofilm layer is in contact with sewer atmosphere and its growth

towards the interior cavity of the pipe is regulated by metabolic growth of SOBs and detachment processes. Gypsum is the product of corrosion, formed from the chemical reaction between acid produced by SOBs and calcium carbonate present in the uncorroded concrete. As in [6], we assume the reaction is fast and complete, consuming all the available calcium carbonate immediately at the interface. Accordingly, the corrosion process is modeled as a localized conversion of concrete into gypsum at $x = L_2(t)$, leading to an expansion of the gypsum layer within the concrete. It's worth noting that the proliferation of SOB biofilms on concrete pipes is typically associated with pH variations that initiate an ecological succession of multiple strains of SOBs [37]. To simplify we do not include here the pH as a model variable. Instead, we group the biofilm community into one single functional class, and employ a kinetic expression that reasonably approximates the overall metabolic activity of SOBs.

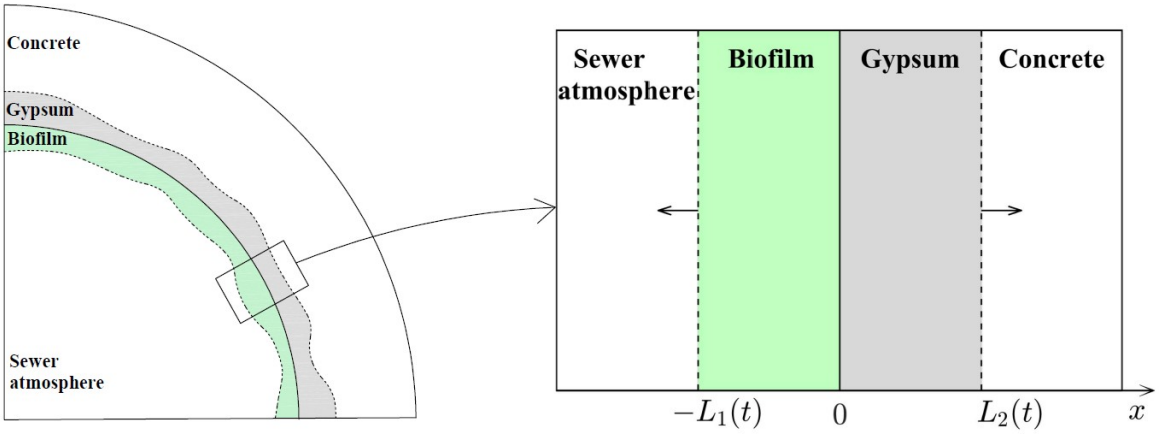

Figure 1. Cross section of the sewer cavity (left). Schematic representation of the model's double free boundary domain (right). The biofilm region, defined for $-L_1(t) \leq x \leq 0$, evolves towards the sewer cavity. The gypsum layer, formed from corrosion and defined for $0 < x \leq L_2(t)$, penetrates the concrete wall. Both layers expand in the x-direction, perpendicular to the biofilm-gypsum interface fixed at $x = 0$.

3.1. Model equations

The model considers the dynamics of three chemical compounds, expressed in terms of concentrations:

- Hydrogen sulfide H_2S, $S_H(x,t)$, $-L_1(t) \leq x \leq 0$, $t \geq 0$.
- Dissolved oxygen O_2, $S_O(x,t)$, $-L_1(t) \leq x \leq 0$, $t \geq 0$.
- Sulfuric acid SO_4^{2-}, $S_A(x,t)$, $-L_1(t) \leq x \leq L_2(t)$, $t \geq 0$.

Notably, hydrogen sulfide and oxygen are not modeled in the gypsum layer as they are presumed to play no direct role in the corrosion process.

A system of parabolic partial differential equations describes the reaction and diffusion transport of chemical compounds within the biofilm layer:

$$\frac{\partial S_A(x,t)}{\partial t} - \alpha_{A,b}\frac{\partial^2 S_A(x,t)}{\partial x^2} = F_A(S_H(x,t), S_O(x,t)), \ -L_1(t) < x < 0, \tag{3.1}$$

$$\frac{\partial S_H(x,t)}{\partial t} - \alpha_{H,b}\frac{\partial^2 S_H(x,t)}{\partial x^2} = F_H(S_H(x,t), S_O(x,t)),\ -L_1(t) < x < 0, \tag{3.2}$$

$$\frac{\partial S_O(x,t)}{\partial t} - \alpha_{O,b}\frac{\partial^2 S_O(x,t)}{\partial x^2} = F_O(S_H(x,t), S_O(x,t)),\ -L_1(t) < x < 0, \tag{3.3}$$

with $t > 0$, where $\alpha_{A,b}$, $\alpha_{H,b}$, $\alpha_{O,b}$ are the diffusivity coefficients of SO_4^{2-}, H_2S, O_2 in the biofilm, respectively. F_A, F_H, F_O denote the conversion rates of SO_4^{2-}, H_2S, O_2, respectively, related to the metabolic growth of SOBs, and are modeled through Monod-type kinetics:

$$F_A = \frac{\mu_{max}}{Y}\frac{S_H}{K_H + S_H}\frac{S_O}{K_O + S_O}X_{SOB}, \tag{3.4}$$

$$F_H = -\frac{\mu_{max}}{Y}\frac{S_H}{K_H + S_H}\frac{S_O}{K_O + S_O}X_{SOB}, \tag{3.5}$$

$$F_O = -\frac{2-Y}{Y}\mu_{max}\frac{S_H}{K_H + S_H}\frac{S_O}{K_O + S_O}X_{SOB}, \tag{3.6}$$

where μ_{max} is the maximum growth rate, Y is the yield of SOBs on H_2S, K_H and K_O are the half-saturation coefficients of hydrogen sulfide and oxygen, respectively. Note that F_H and F_O are negative and represent the consumption of hydrogen sulfide and oxygen while F_A is positive and denotes the production of sulfuric acid. Notably, $-\frac{2-Y}{Y}$ represents the stoichiometric coefficient for oxygen, derived according to stoichiometric considerations related to chemical reaction (2.1).

A homogeneous parabolic equation governs the diffusion of SO_4^{2-} in the gypsum layer:

$$\frac{\partial S_A(x,t)}{\partial t} - \alpha_{A,g}\frac{\partial^2 S_A(x,t)}{\partial x^2} = 0,\ 0 < x < L_2(t),\ t > 0, \tag{3.7}$$

where $\alpha_{A,g}$ denotes the diffusivity coefficient of SO_4^{2-} within the gypsum layer.

The time evolution of the gypsum free boundary $L_2(t)$, which also represents the corrosion front, is modeled using a semi-empirical approach, consistent with the works of [6, 7, 31]. We assume here that $\dot{L}_2(t)$ is proportional to the rate of calcium carbonate consumption associated with the corrosion reaction (2.2), expressed as $F_C K_C S_A(L_2(t), t)$, where K_C denotes the dissolution rate constant. Since S_A is expressed in grams, the molar mass ratio between $CaCO_3$ and SO_4^{2-}, given by $F_C = 1.04$, is incorporated into the formulation. Furthermore, it is reasonable to expect that higher concentrations of calcium carbonate in concrete, C_C, impede the progression of the reaction front, indicating an inverse dependence. Combining these assumptions yields the following relation:

$$\dot{L}_2(t) = \frac{F_C K_C}{C_C} S_A(L_2(t), t),\ t > 0. \tag{3.8}$$

An equivalent interpretation of Eq (3.8) is that the product $C_C\dot{L}_2(t)$ represents the mass of calcium carbonate consumed per unit time, which corresponds to the aforementioned consumption rate $K_C S_A(L_2(t), t)$, adjusted by the conversion factor F_C.

The thickness of the biofilm layer $L_1(t)$, on the other hand, is governed by the following equation, derived from a global mass balance on the biofilm domain [51]:

$$-\dot{L}_1(t) = U(t) - \sigma(L_1(t)),\ t > 0, \tag{3.9}$$

where $U(t)$ is the biofilm velocity, induced by the overall growth processes of SOBs in the biofilm

$$U(t) = \int_{-L_1(t)}^{0} \mu_{max} \frac{S_H}{K_H + S_H} \frac{S_O}{K_O + S_O} dx, \ t \geq 0, \tag{3.10}$$

and $\sigma(L_1(t))$ is the detachment velocity, accounting for phenomena of biomass loss, modelled as a quadratic function of biofilm thickness [51]:

$$\sigma(L_1(t)) = \lambda L_1(t)^2, \tag{3.11}$$

with λ representing the detachment coefficient, that accounts for erosion phenomena induced by external stressors. Formulation (3.11) reflects a widely adopted detachment criterion in biofilm modeling [1]. In particular, it captures the experimentally observed behavior of thicker biofilms to exhibit higher detachment rates due to increased shear stress exposure [50], while also supporting the emergence of a steady-state biofilm thickness [11, 45].

3.2. Initial and boundary conditions

The biocorrosion problem is described by Eqs (3.1)–(3.3) and (3.7)–(3.9). The following initial conditions are considered for Eqs (3.1)–(3.3) and (3.7):

$$S_A(x, 0) = S_{A,0}(x) \qquad -L_1(0) \leq x \leq L_2(0), \tag{3.12}$$

$$S_H(x, 0) = S_{H,0}(x) \qquad -L_1(0) \leq x \leq 0, \tag{3.13}$$

$$S_O(x, 0) = S_{O,0}(x) \qquad -L_1(0) \leq x \leq 0. \tag{3.14}$$

Dirichlet prescribed conditions on the biofilm free boundary $x = -L_1(t)$ (sewer atmosphere-biofilm interface) ensure an infinite reservoir of hydrogen sulfide and oxygen

$$S_H(-L_1(t), t) = S_{H,L_1}(t), \ t > 0, \tag{3.15}$$

$$S_O(-L_1(t), t) = S_{O,L_1}(t), \ t > 0, \tag{3.16}$$

while homogeneous Neumann conditions (null flux) are set at biofilm-gypsum interface $x = 0$

$$\frac{\partial S_H}{\partial x}(0, t) = 0, \ t > 0, \tag{3.17}$$

$$\frac{\partial S_O}{\partial x}(0, t) = 0, \ t > 0. \tag{3.18}$$

For sulfuric acid, a Robin boundary condition is prescribed on the biofilm free boundary $x = -L_1(t)$, assuming a leak of sulfuric acid, regulated by the rate h_a, due to physical factors such as gravity

$$\alpha_{A,b} \frac{\partial S_A(L_1(t), t)}{\partial x} = h_a S_A(L_1(t), t), \ t > 0. \tag{3.19}$$

At biofilm-gypsum interface, we impose continuity conditions for both the concentration and flux of sulfuric acid:

$$S_A(0^-, t) = S_A(0^+, t), \ t > 0, \tag{3.20}$$

$$\alpha_{A,b}\frac{\partial S_A(0^-,t)}{\partial x} = \alpha_{A,g}\frac{\partial S_A(0^+,t)}{\partial x},\ t>0. \tag{3.21}$$

A second Robin boundary condition is considered at the gypsum-concrete interface $x = L_2(t)$, modeling a consumption of acid, regulated by the dissolution constant rate K_C, due to the chemical reaction with calcium carbonate

$$\alpha_{A,g}\frac{\partial S_A(L_2(t),t)}{\partial x} = -K_C S_A(L_2(t),t),\ t>0. \tag{3.22}$$

It is worth noting that, based on relation (3.22), Eq (3.8) can alternatively be expressed in the more conventional form:

$$\dot{L}_2(t) = -\frac{F_C\alpha_{A,g}}{C_c}\frac{\partial S_A(L_2(t),t)}{\partial x},\ t>0. \tag{3.23}$$

Finally, Eqs (3.8) and (3.9) regulate the evolution of two free boundaries over time, and are associated with the following initial conditions:

$$L_1(0) = L_{1,0}, \tag{3.24}$$

$$L_2(0) = L_{2,0}. \tag{3.25}$$

4. Results and discussion

The model is integrated by developing an in-house MATLAB code. The multilayer domain is discretized using two distinct, uniform spatial mesh grids for the biofilm and gypsum layers. The element sizes adjust over time according to the evolving free boundaries. Diffusion-reaction equations (3.1)–(3.3) and (3.7) are solved through the method of lines, a well-established numerical method for solving boundary value problems for parabolic PDEs in one spatial dimension [16]. The free boundary equations (3.8) and (3.9) are addressed using the finite differences method, and boundary conditions (3.19) and (3.22) are approximated through three-point discretizations. The target simulation time is 365 days, corresponding to computational times in the order of days.

We conducted numerical studies to examine the behavior of the model. Section 4.1 present an illustrative simulation, depicting key aspects of the biocorrosion process, including the formation and evolution of the biofilm and the subsequent progression of corrosion. Sections 4.2–4.4 feature simulations varying significant parameters to study their effects on the process. Specifically, Section 4.2 investigates the process for different H_2S levels in the pipeline and Section 4.3 for different calcium carbonate concentrations in the concrete C_C. Finally, Section 4.4 analyzes the effects of the detachment coefficient λ, the diffusivity of sulfuric acid in gypsum $\alpha_{A,g}$, and the acid leak rate h_a on the model outcome.

All model parameters are listed in Table 1. The concentration of O_2 at the sewer atmosphere-biofilm boundary is assumed equal to the saturation value in water, while the concentration of H_2S in the pipeline and the concentration of $CaCO_3$ in concrete C_C are set in the range of typical values observed in wastewater pipes [7, 38]. The detachment coefficient λ is selected to achieve a biofilm thickness within the range of values reported in the literature [35]. Diffusion in biofilm is assumed to be 80% of the diffusivity in water, in accordance with [51]. Initial biofilm and gypsum thicknesses are

fixed at 100 μm. The initial concentrations of O_2 and H_2S, $S_{O,0}$ and $S_{H,0}$, are set equal to the values at the biofilm free boundary, while the initial concentration of SO_4^{2-}, $S_{A,0}$, is set to zero.

Table 1. Model parameters and boundary values.

Parameter	Definition	Unit	Value	Ref
μ_{max}	Maximum growth rate	1.3	$1/d$	[19]
K_H	H_2S half saturation coefficient	0.032	g/m^3	[36]
K_O	O_2 half saturation coefficient	0.1	g/m^3	[18]
Y	Yield of SOB on H_2S	0.2	g/g	[28]
X_{SOB}	SOB microbial density	5000	g/m^3	[51]
K_C	Dissolution constant rate	8.08	m/d	[7]
α_H	Diffusion coefficient of H_2S in biofilm	$1.1 \cdot 10^{-4}$	m^2/d	[46]
α_O	Diffusion coefficient of O_2 in biofilm	$1.75 \cdot 10^{-4}$	m^2/d	[40]
$\alpha_{A,b}$	Diffusion coefficient of SO_4^{2-} in biofilm	$7.3 \cdot 10^{-5}$	m^2/d	[42]
$\alpha_{A,g}$	SO_4^{2-} Diffusion coefficient of SO_4^{2-} in gypsum	$[1 \cdot 10^{-6} - 1 \cdot 10^{-3}]$	m^2/d	Varied
C_C	Calcium carbonate concentration	[20000 – 100000]	g/m^3	Varied
λ	Detachment coefficient	[50 – 20000]	$1/m/d$	Varied
h_a	Acid leak rate	[0.05 – 10]	m/d	Varied
S_{H,L_1}	Concentration of H_2S at the biofilm free boundary $L_1(t)$	[0.16 – 0.80]	g/m^3	Varied
S_{O,L_1}	Concentration of O_2 at the biofilm free boundary $L_1(t)$	9.81	g/m^3	Assumed

4.1. Illustrative simulation

In this section we investigate the dynamics of biofilm growth and corrosion advancement, showcasing the main aspects of the biocorrosion process. Results are reported in Figures 2–4.

Figure 2 illustrates the growth of the biofilm (left) and the advancement of the corrosion front against t (middle) and $\sqrt{t}$ (right). As can be seen, the evolution of the biofilm thickness $L_1(t)$ is marked by two distinct phases. It increases linearly during the first 20–30 days. Later on, detachment phenomena intensify, proportionally to $L_1(t)$, leading to a steady-state biofilm thickness of approximately 1 mm, which is consistent with typical values reported in experimental studies [24]. This is a characteristic behavior observed in the biofilm development process [20]. On the other hand, the gypsum layer, tracked by the free boundary $L_2(t)$, continues to expand indefinitely, achieving a thickness of approximately 3 mm within a year, consistent with the range of values reported in literature [23, 30, 32, 38, 53]. Similar to biofilm development, the corrosion process exhibits two distinct phases. In the initial phase, when the biofilm is still growing, $L_2(t)$ advances more rapidly. This is followed by a second phase, starting around 50 to 100 days, in which the biofilm has reached its steady-state thickness and the progression of $L_2(t)$ approaches a $\sqrt{t}$ behavior. This latter trend aligns well with a wide range of modeling [2, 10] and experimental [27, 39] results available in the literature.

Figure 3 shows the evolution of the corrosion rate over time. Initially, the corrosion velocity is at its maximum and decreases as the biofilm-gypsum system thickness increases. This trend shows a steeper linear decline in the first days, coinciding with the growth of the biofilm, while a sharp reduction in slope is observed when the biofilm reaches its steady state, in line with the behavior observed in Figure 2.

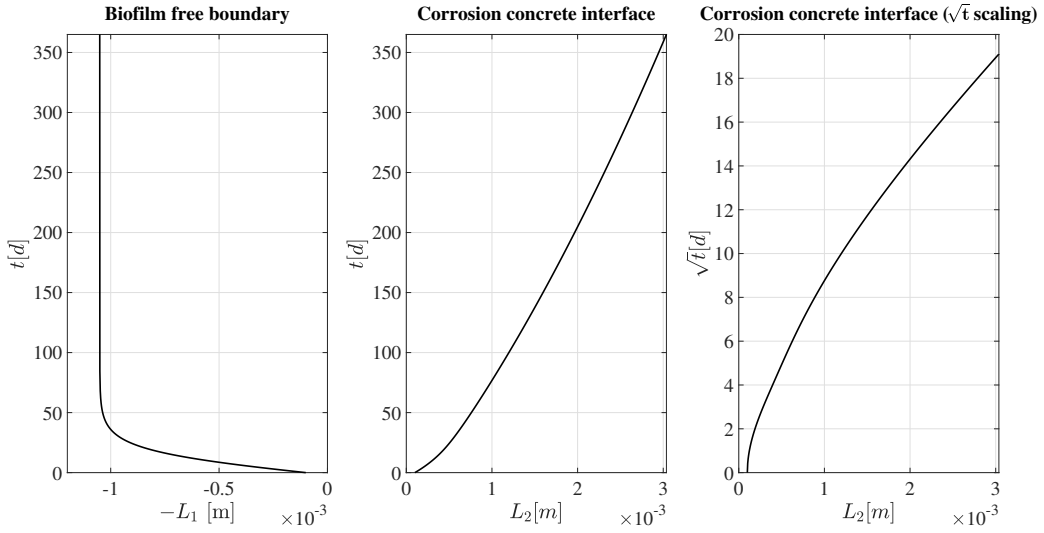

Figure 2. Time evolution of biofilm thickness $L_1(t)$ (left), and corrosion concrete interface $L_2(t)$ plotted against t (middle) and $\sqrt{t}$ (right). The biofilm-gypsum interface is fixed at $x = 0$. $C_C = 50000\ g\ m^{-3}$, $S_{H,L_1} = 0.31\ g\ m^{-3}$, $\alpha_{A,g} = 10^{-4}\ m^2\ d^{-1}$, $\lambda = 50\ m^{-1}\ d^{-1}$, $h_a = 0.05\ m\ d^{-1}$.

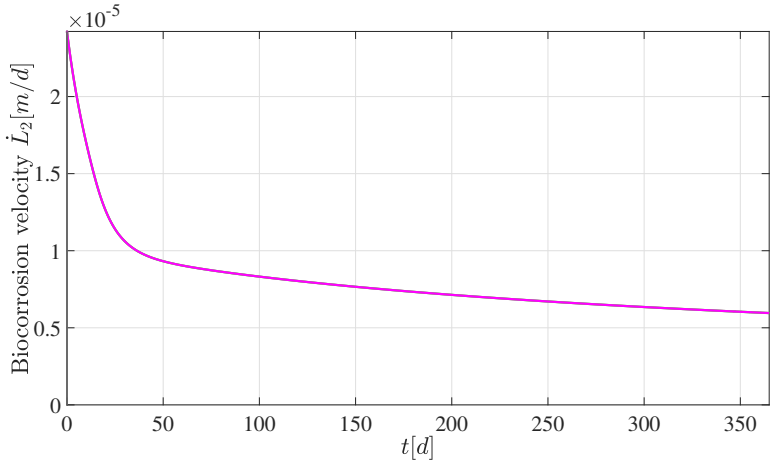

Figure 3. Time evolution of the biocorrosion rate. $C_C = 50000\ g\ m^{-3}$, $S_{H,L_1} = 0.31\ g\ m^{-3}$, $\alpha_{A,g} = 10^{-4}\ m^2\ d^{-1}$, $\lambda = 50\ m^{-1}\ d^{-1}$, $h_a = 0.05\ m\ d^{-1}$.

These findings point to an important conclusion: In thicker biofilm-gypsum systems, the intensified diffusion limitation significantly reduces acid availability at the gypsum-concrete interface, resulting in a slower corrosion process. This effect, and its implications for long-term durability, will be further examined in an upcoming numerical investigation.

The concentration profiles of H_2S (top-left) and O_2 (top-right) in the biofilm and SO_4^{2-} in the biofilm-gypsum system (bottom) are depicted in Figure 4. O_2 and H_2S present their maximum levels at the sewer atmosphere-biofilm interface and exhibit a decreasing trend across the biofilm, primarily due to consumption by SOBs. Specifically, the concentration of H_2S decreases significantly in the outermost

layers until reaching zero, while oxygen remains at high levels throughout the biofilm. This suggests that the metabolic process of SOBs is constrained by the concentration of H_2S in the inner layers of the biofilm. This metabolic process also results in the production of SO_4^{2-} in the outer region of the biofilm, which diffuses towards the gypsum layer and the corrosion front. The concentration of SO_4^{2-} decreases with increasing depth due to diffusion limitation and consumption at the gypsum-concrete interface. Note the slight decrease in acid concentration near the sewer atmosphere-biofilm interface, attributed to mass leaks occurring at that interface.

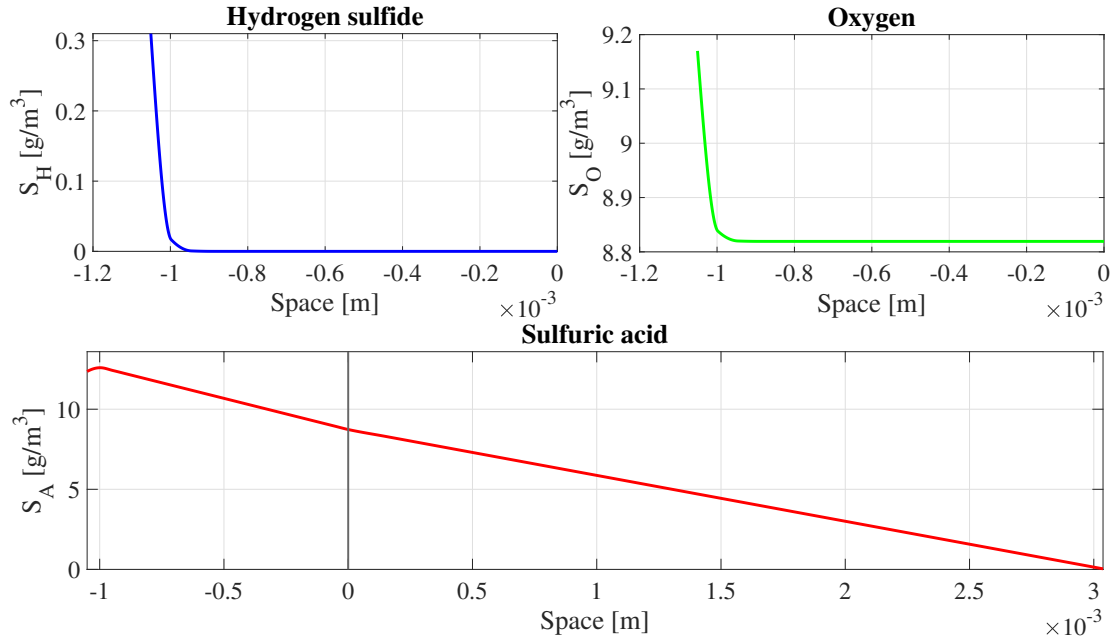

Figure 4. (Top) Concentration profile of H_2S (left) and O_2 (right) within the biofilm at $t = 365\ d$. (Bottom) Concentration profile of SO_4^{2-} within the biofilm-gypsum system at $t = 365\ d$. The biofilm-gypsum interface is set at $x = 0$. $C_C = 50000\ g\ m^{-3}$, $S_{H,L_1} = 0.31\ g\ m^{-3}$, $\alpha_{A,g} = 10^{-4}\ m^2\ d^{-1}$, $\lambda = 50\ m^{-1}\ d^{-1}$, $h_a = 0.05\ m\ d^{-1}$.

4.2. Effect of hydrogen sulfide level on biocorrosion

The severity of biocorrosion in wastewater pipes is frequently correlated with the presence of hydrogen sulfide. Elevated levels of H_2S can lead to large acid production, and accelerate the deterioration of pipes. To assess the impact of H_2S on the corrosion process, we carried out numerical simulations across a range of concentrations of H_2S at the biofilm free boundary $L_1(t)$, S_{H,L_1}, encompassing the typical range found in wastewater pipes ($0.16 - 0.8\ g/m^3$) [38]. The numerical results are presented in Figures 5 and 6.

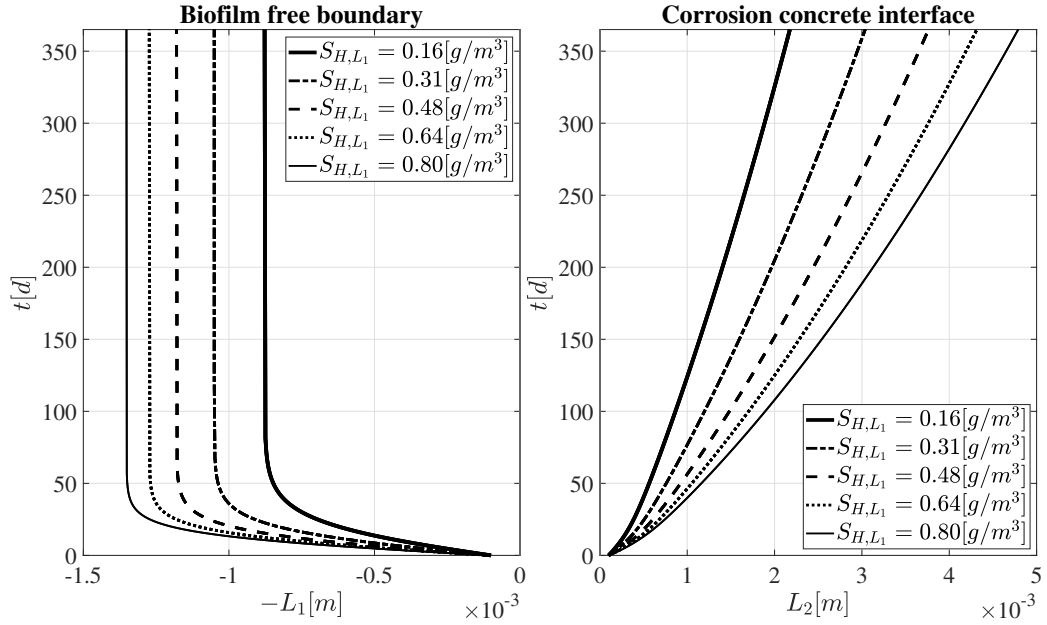

Figure 5. Time evolution of biofilm thickness $L_1(t)$ (left) and corrosion concrete interface $L_2(t)$ (right), for different hydrogen sulfide levels S_{H,L_1}. The biofilm-gypsum interface is set at $x = 0$. $C_C = 50000\ g\ m^{-3}$, $\alpha_{A,g} = 10^{-4}\ m^2\ d^{-1}$, $\lambda = 50\ m^{-1}\ d^{-1}$, $h_a = 0.05\ m\ d^{-1}$.

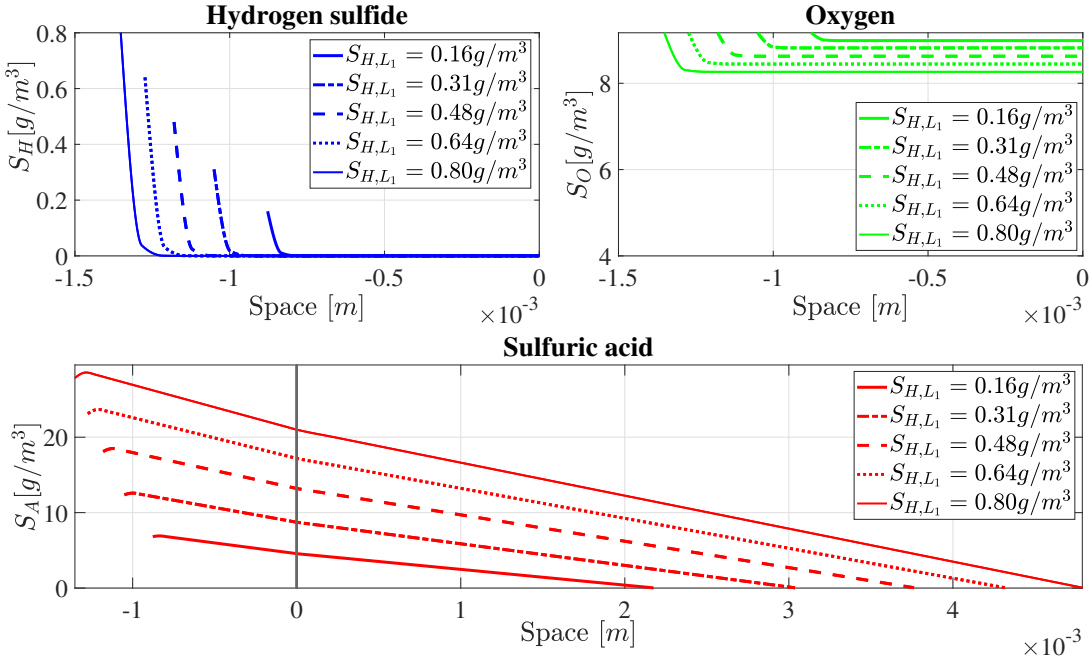

Figure 6. (Top) Concentration profile of H_2S (left) and O_2 (right) within the biofilm at $t = 365\ d$, for different hydrogen sulfide levels S_{H,L_1}. (Bottom) Concentration profile of SO_4^{2-} within the biofilm-gypsum system at $t = 365\ d$, for different concentrations of S_{H,L_1}. The biofilm-gypsum interface is set at $x = 0$. $C_C = 50000\ g\ m^{-3}$, $\alpha_{A,g} = 10^{-4}\ m^2\ d^{-1}$, $\lambda = 50\ m^{-1}\ d^{-1}$, $h_a = 0.05\ m\ d^{-1}$.

Figure 5 illustrates how hydrogen sulfide at the boundary S_{H,L_1} affects the evolution of the biofilm thickness (left) and gypsum-concrete interface (right). As expected, higher levels of hydrogen sulfide at the boundary result in thicker biofilms and faster corrosion. It is noteworthy that while S_{H,L_1} affects the steady-state biofilm thickness, it does not impact the time required to reach this state. The influence of S_{H,L_1} on the corrosion front is further revealed when observing how it impacts the concentration profiles of substrates, reported in Figure 6. These profiles display consistent qualitative trends, yet quantitative differences. Specifically, a higher concentration of hydrogen sulfide at the boundary leads to more intense metabolic processes by SOBs, consequently resulting in greater oxygen consumption and increased acid production, which directly governs the corrosion progression.

In all simulations, oxygen consistently maintains high concentrations throughout the biofilm compared to the related half saturation constant. This suggests that the main limiting substrate is hydrogen sulfide while oxygen does not restrict or impede the microbial growth process. Notably, when combined with the availability of other nutrients like organic carbon and ammonium, such high oxygen levels may promote the emergence of alternative aerobic metabolic pathways not accounted for in our model, such as those associated with heterotrophic and nitrifying bacteria [24].

4.3. Effect of calcium carbonate concentration on biocorrosion

As explained in Section 2, the corrosion process in carbonated concrete pipes is driven by sulfuric acid produced within the biofilm reacting with calcium carbonate. Hence, the propagation of the corrosion front is strongly related to the calcium carbonate concentration in the concrete C_C. In this context, different simulations have been conducted to examine the effect of C_C on the model output. C_C has been varied within the range of values provided in the literature [6, 7]. Results are shown in Figures 7–9.

Figure 7 illustrates the progression of the biofilm thickness (left) and the corrosive front (right) over time, for different C_C values. The evolution of the corrosion front exhibits notable sensitivity to changes in C_C. In particular, higher concentrations of calcium carbonate in the concrete lead to a slower progression of the corrosion front. This correlation is also evident from Eq (3.8). Remarkably, the concentration of calcium carbonate solely influences the corrosion process, with no impact on biofilm growth dynamics.

Figure 8 offers insights into the concentration profiles of sulfuric acid within the biofilm-gypsum domain at $t = 365\ d$, for different C_C values. These profiles display similar qualitative trends but differ quantitatively: Increased C_C values result in greater acid consumptions per unit of volume, consequently leading to lower acid concentrations throughout the system. Note that, as previously mentioned, variations in calcium carbonate concentration do not impact the biofilm growth dynamics and, consequently, the consumption of hydrogen sulfide and oxygen, whose concentration trends remain unaffected by C_C (data not shown).

Finally, an overview of the combined effect of S_{H,L_1} and C_C on the corrosion thickness is provided in Figure 9.

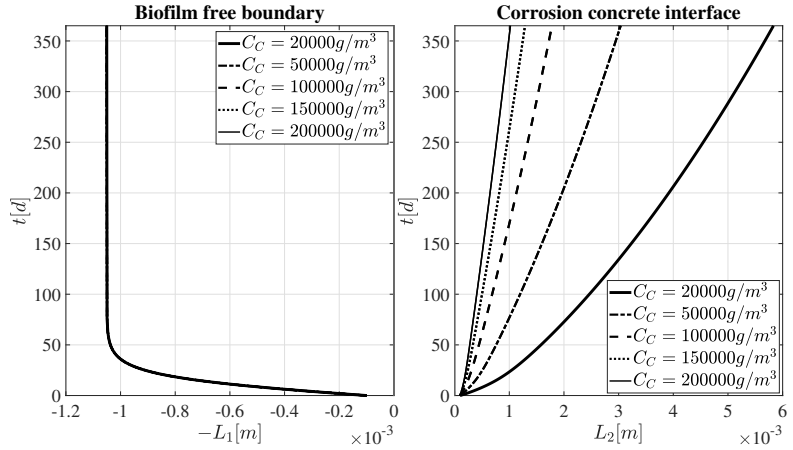

Figure 7. Time evolution of biofilm thickness $L_1(t)$ (left) and corrosion concrete interface $L_2(t)$ (right), for different concentrations of calcium carbonate C_C. The biofilm-gypsum interface is set at $x = 0$. $S_{H,L_1} = 0.31\ g\ m^{-3}$, $\alpha_{A,g} = 10^{-4}\ m^2\ d^{-1}$, $\lambda = 50\ m^{-1}\ d^{-1}$, $h_a = 0.05\ m\ d^{-1}$.

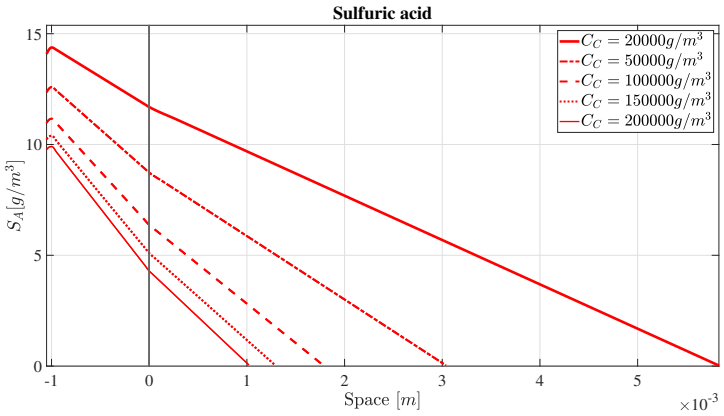

Figure 8. Concentration profile of SO_4^{2-} within the biofilm-gypsum system at $t = 365\ d$, for different concentrations of calcium carbonate C_C. The biofilm-gypsum interface is set at $x = 0$. $S_{H,L_1} = 0.31\ g\ m^{-3}$, $\alpha_{A,g} = 10^{-4}\ m^2\ d^{-1}$, $\lambda = 50\ m^{-1}\ d^{-1}$, $h_a = 0.05\ m\ d^{-1}$.

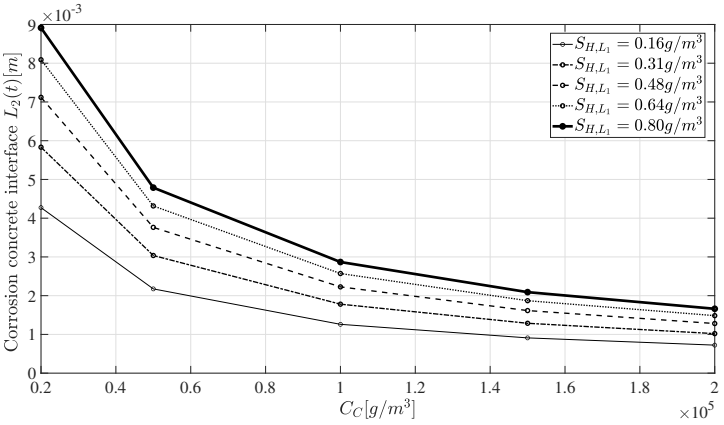

Figure 9. Corrosion thickness at $t = 365\ d$ for different concentrations of calcium carbonate C_C and different hydrogen sulfide levels S_{H,L_1}. $\alpha_{A,g} = 10^{-4}\ m^2\ d^{-1}$, $\lambda = 50\ m^{-1}\ d^{-1}$, $h_a = 0.05\ m\ d^{-1}$.

4.4. *Effect of λ, $\alpha_{A,g}$ and h_a on biocorrosion*

We conduce here further numerical studies with a specific focus on parameters associated with high uncertainty.

Detachment phenomena in wastewater pipes are affected by a range of factors including human activity, weather conditions, shear forces, and hydraulic load. The influence of all these factors is included in the model through the detachment coefficient λ, whose value is consequently associated with a high level of uncertainty. To assess the impact of this parameter on the model output, we performed simulations for different λ values. Results are shown in Figures 10–12.

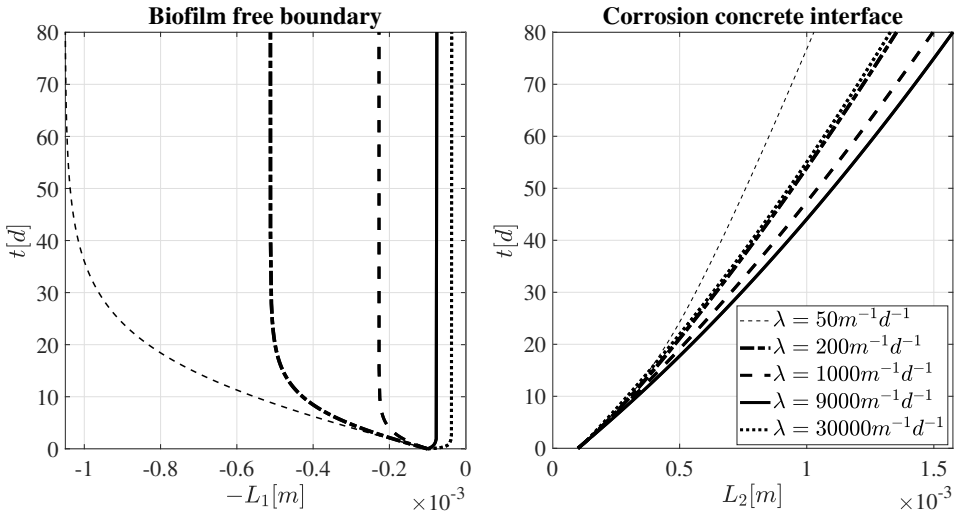

Figure 10. Time evolution of biofilm thickness $L_1(t)$ (left) and corrosion concrete interface $L_2(t)$ (right), for different values of the detachment coefficient λ. The biofilm-gypsum interface is set at $x = 0$. $C_C = 50000\ g\ m^{-3}$, $S_{H,L_1} = 0.31\ g\ m^{-3}$, $\alpha_{A,g} = 10^{-4}\ m^2\ d^{-1}$, $h_a = 0.05\ m\ d^{-1}$.

Figure 10 depicts the spatial evolution of the biofilm-gypsum domain. A more intense detachment (higher λ value) results in thinner steady-state biofilms. On the other hand, the effect of λ on the corrosion thickness is not straightforward. This is further highlighted in Figure 11, where the corrosion thickness is shown at $t = 100\ d$ as λ varies. This outcome can be elucidated by considering the diffusion-reaction dynamics of substrates. Acid production by SOBs only occurs in the outermost region of the biofilm, where hydrogen sulfide is not limiting (see Figure 4). Elevated λ values result in thinner steady-state biofilms, causing the acid production region to shift closer to the uncorroded concrete wall. As a result of reduced diffusion limitation, a greater amount of acid reaches the concrete interface, leading to faster corrosion. However, for extremely high values of λ, the corrosion rate slows down. This likely occurs when the steady-state biofilm becomes so thin that its entire thickness is smaller than the potential acid production region, thereby diminishing overall acid production. In light of this result, the model suggests an interesting conclusion. The maximum intensity of the corrosion phenomenon is reached when the steady-state biofilm thickness coincides with the thickness of the acid production region. A thinner biofilm may lead to an overall lower production of acid, resulting in a slowdown of the phenomenon. Conversely, a thicker biofilm may play a protective role by imposing limitations on the acid diffusion towards the concrete interface.

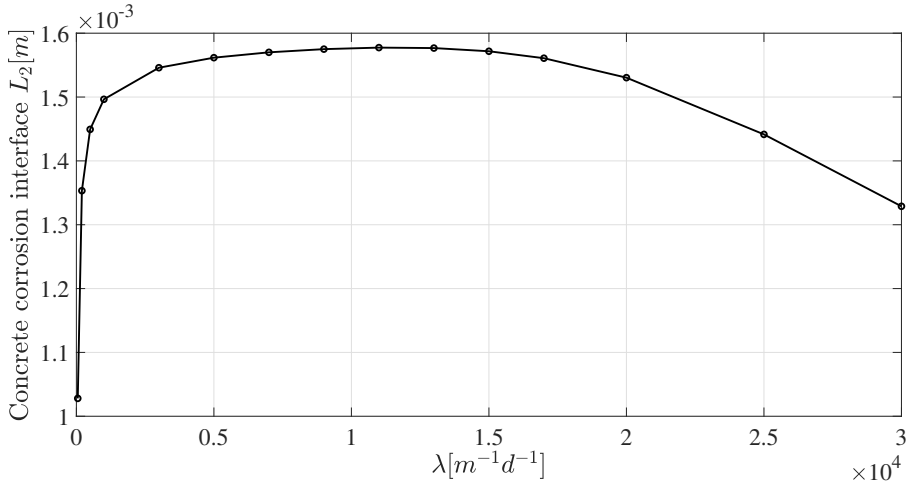

Figure 11. Corrosion thickness at $t = 100\ d$ for different values of the detachment coefficient λ. $C_C = 50000\ g\ m^{-3}$, $S_{H,L_1} = 0.31\ g\ m^{-3}$, $\alpha_{A,g} = 10^{-4}\ m^2\ d^{-1}$, $h_a = 0.05\ m\ d^{-1}$.

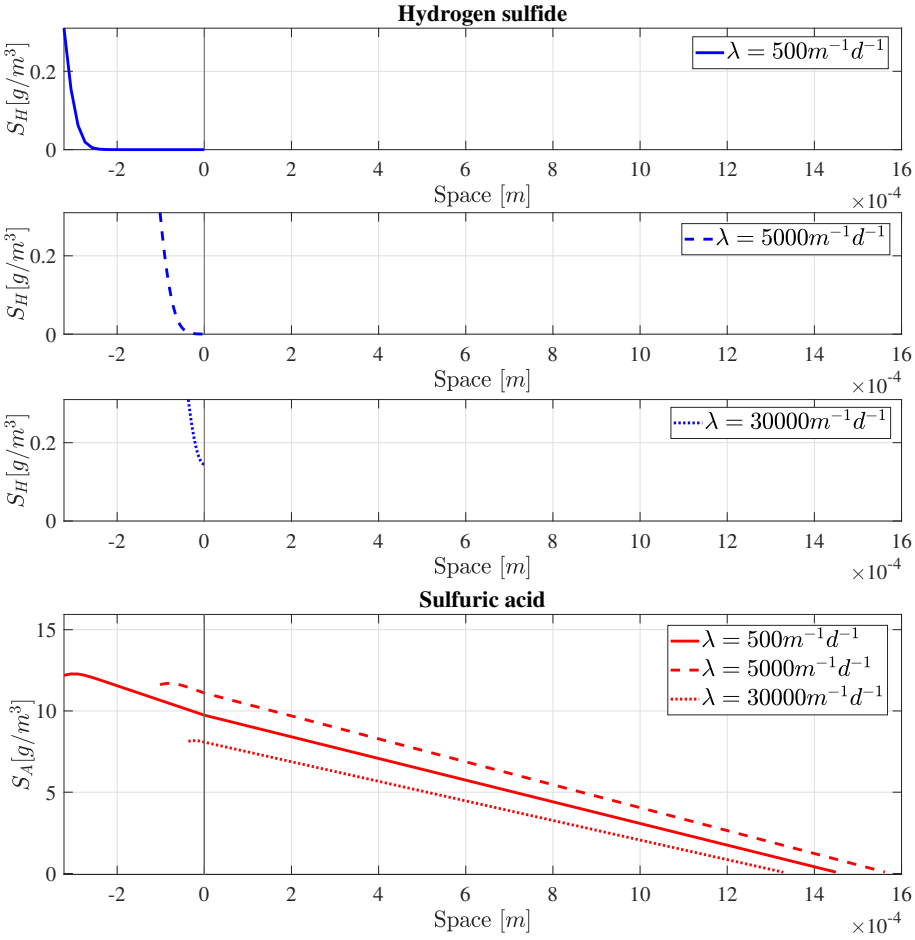

Figure 12. Concentration profile of H_2S within the biofilm (in blue) and SO_4^{2-} within the biofilm-gypsum system (in red), at $t = 100\ d$, for different values of the detachment coefficient λ. The biofilm-gypsum interface is set at $x = 0$. $C_C = 50000\ g\ m^{-3}$, $S_{H,L_1} = 0.31\ g\ m^{-3}$, $\alpha_{A,g} = 10^{-4}\ m^2\ d^{-1}$, $h_a = 0.05\ m\ d^{-1}$.

In support of this, Figure 12 reports the profiles of hydrogen sulfide and sulfuric acid across three distinct values of λ which thoroughly describe this behavior. Importantly, the extent of the acid production region is strongly influenced by the hydrogen sulfide concentration in the pipeline, leading to a complex interplay between biofilm thickness, substrate availability, and acid generation, which ultimately governs the dynamics of the corrosion process. This finding serves as a perfect illustration of the importance of accounting for the spatial description of the microbial aggregate when dealing with biofilm-induced phenomena.

Significant uncertainty is also associated with the acid diffusion coefficient within the gypsum layer $\alpha_{A,g}$. The gypsum layer may be composed by various corrosion products and exhibit varying porosity, posing challenges in determining its diffusion properties. In light of this, simulations were conducted by varying $\alpha_{A,g}$, with the results depicted in Figure 13. The obtained results suggest that an increased diffusivity within the gypsum layer may markedly accelerates the progression of acid towards the uncorroded interface, thereby fostering the corrosion process. Notably, the thickness of the biofilm layer remains unaffected by $\alpha_{A,g}$, as the latter does not influence the biofilm dynamics.

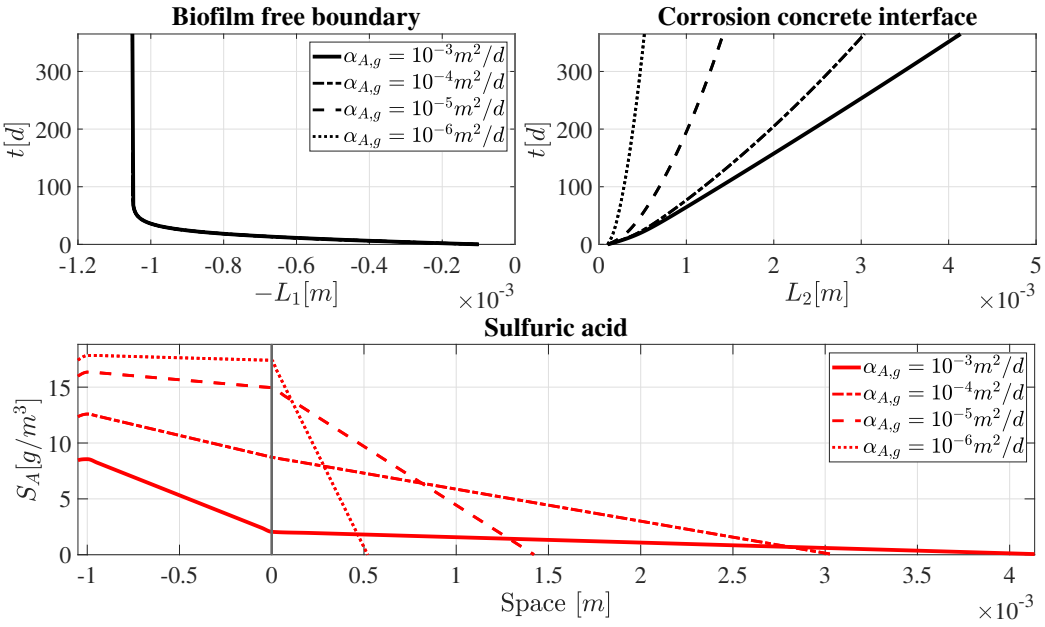

Figure 13. (Top) Time evolution of biofilm thickness $L_1(t)$ (left) and corrosion concrete interface $L_2(t)$ (right), for different values of $\alpha_{A,g}$. (Bottom) Concentration profile of SO_4^{2-} within the biofilm-gypsum system at $t = 365\ d$, for different values of $\alpha_{A,g}$. The biofilm-gypsum interface is set at $x = 0$. $C_C = 50000\ g\ m^{-3}$, $S_{H,L_1} = 0.31\ g\ m^{-3}$, $\lambda = 50\ m^{-1}\ d^{-1}$, $h_a = 0.05\ m\ d^{-1}$.

Lastly, we performed simulations for different acid leak rates at the sewer atmosphere-biofilm interface h_a. Determining this parameter value presents challenges due to its dependence on various factors, such as biofilm properties, the biofilm's position within the sewer, and airflow dynamics. As can be seen in Figure 14, the influence of h_a on the corrosion process seems substantial. With increasing h_a, the residual acid concentration in the system diminishes, resulting in a reduced corrosion process. This could explain the occurrence of localized hotspots of corrosion in concrete wastewater

pipes [17, 44], in regions where specific local conditions might mitigate acid leaks leading to more intense corrosive reactions on the concrete surface. Furthermore, it should be noted that the acid leaked from the reference domain could induce corrosive phenomena on different regions of the concrete surface, even those not affected by biofilms.

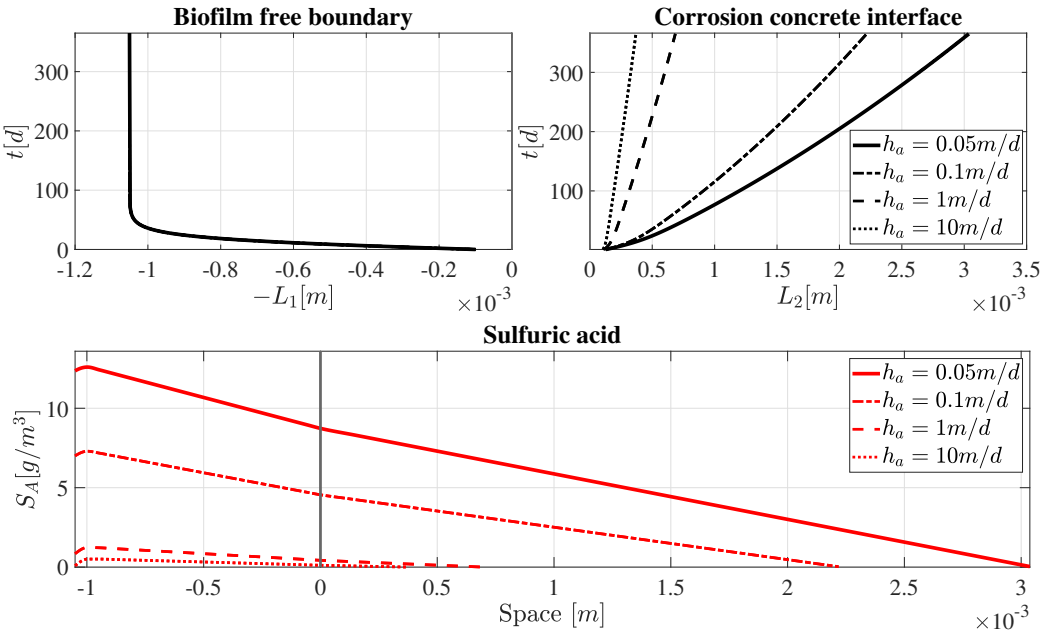

Figure 14. (Top) Time evolution of biofilm thickness $L_1(t)$ (left) and gypsum thickness $L_2(t)$ (right), for different acid leak rates h_a. (Bottom) Concentration profile of SO_4^{2-} within the biofilm-gypsum system at $t = 365\ d$, for different acid leak rates h_a. The biofilm-gypsum interface is set at $x = 0$. $C_C = 50000\ g\ m^{-3}$, $S_{H,L_1} = 0.31\ g\ m^{-3}$, $\alpha_{A,g} = 10^{-4}\ m^2\ d^{-1}$, $\lambda = 50\ m^{-1}\ d^{-1}$.

5. Conclusions

This study proposes a model aimed at describing the biocorrosion process in concrete sewer pipes, induced by the proliferation of SOB biofilm colonies and the related production of sulfuric acid. For the first time, this process is modeled including the biofilm spatial dynamics and the microbially-induced corrosion of concrete, through the formulation of a double free boundary problem within a one-dimensional two-layer domain, which accounts for biofilm and gypsum components.

The numerical results provide valuable insights into the dynamics of biofilm growth and corrosion advancement over time. The biofilm growth exhibits two distinct phases: An initial linear intense growth until reaching a steady-state configuration induced by detachment phenomena. Conversely, the gypsum layer shows indefinite growth, indicating continuous corrosion progression. The corrosion process also displays two phases: Initially, the corrosion velocity is at its maximum and shows a rapid linear decline as the biofilm thickness increases, followed by a sharp reduction in slope when the biofilm reaches its steady-state configuration. This decrease in corrosion velocity can be attributed to diffusion limitations of acid in thicker biofilm-gypsum systems, resulting in lower acid concentrations

at the gypsum-concrete interface.

We performed different numerical studies to explore the dynamics of biofilm and corrosion advancement, assessing the impact of important factors such as hydrogen sulfide concentration in the sewer, calcium carbonate concentration in concrete, detachment phenomena, diffusion of acid in the gypsum layer, and acid leak rate at the sewer atmosphere-biofilm interface. These factors play a crucial role in the biocorrosion process and understanding their effects is essential for formulating efficient strategies to mitigate biocorrosion in wastewater pipes. The presence of hydrogen sulfide in wastewater pipes turns out to be a determining factor for the occurrence of biocorrosion phenomena. The numerical results shows that higher levels of hydrogen sulfide in the sewer atmosphere intensify the metabolic processes of SOBs and lead to thicker biofilms and faster corrosion. The corrosion process is significantly influenced by the calcium carbonate concentration in concrete. Higher concentrations of calcium carbonate result in greater acid consumption per unit of space, leading to a slower advancement of the corrosion front. Furthermore, the model suggests that elevated diffusion of acid in the gypsum layer enhances acid concentration at the concrete interface, thereby speeding up corrosion. Simulations across different acid leak rate values highlight its substantial impact on the corrosion process, with higher rates leading to reduced corrosion due to decreased acid concentration within the system. The acid leak rate may also play a role in the localization of corrosion hotspots experimentally observed in concrete wastewater pipes.

Finally, the model results suggest that biofilms may play a complex dual role in the system by regulating mass transport processes. Specifically, thinner biofilms reduce diffusion limitations, allowing more sulfuric acid to reach the concrete surface and accelerating corrosion. In contrast, thicker biofilms impose stronger diffusion barriers, limiting the acid flux toward the concrete and thus slowing the corrosion process. However, when the biofilm becomes extremely thin, its overall capacity for acid production diminishes, ultimately reducing corrosion despite the lower diffusion resistance. These insights highlight the importance of considering both biofilm thickness and spatially dependent transport phenomena when assessing microbially induced corrosion and may have practical implications for developing strategies to improve the durability and service life of concrete wastewater infrastructure.

To specifically target the corrosion phenomenon and its key contributing factors, we limited our model to a single functional group, sulfur-oxidizing bacteria. This assumption appears to be reasonable for biofilms exposed to the sewer atmosphere, where nutrients like organic carbon and nitrogen are often limited and SOBs tend to dominate [24]. In contrast, these substrates play a much more prominent role in submerged biofilms, where their higher concentrations can support the development of alternative aerobic and anaerobic metabolic pathways – including those involving heterotrophic and nitrifying bacteria – and lead to the production of harmful gaseous compounds [24]. These microbial interactions can include cooperative behaviors that significantly influence population growth and community dynamics [9]. In light of this, expanding the model to include interacting microbial groups and deeper characterize the gas phase [4, 26] would be a valuable direction for future research, offering a more comprehensive view of microbial dynamics in sewer systems.

Future perspectives may also involve the calibration and validation of the present mathematical model through comparison with experimental data. Importantly, while our current modeling approach adequately describes the general aspects of biocorrosion of concrete, a more detailed biochemical description of the biofilm system, including pH modeling and the integration of multispecies biofilm

dynamics, could provide further insights into biofilm ecology and dynamics. Furthermore, a valuable extension of the model could involve accounting for swelling phenomena and concrete heterogeneity to achieve a more detailed representation of the concrete compartment.

Use of Generative-AI tools declaration

The authors declare they have not used Artificial Intelligence (AI) tools in the creation of this article.

Acknowledgments

Alberto Tenore is supported by the co-financing of the European Union-FSE-REACT-EU, PON Research and Innovation 2014–2020, DM 1062/202.

Luigi Frunzo acknowledges support from the project MUR-PRIN 2022 titled "MOMENTA - Modelling complex biOlogical systeMs for biofuEl productioN and sTorAge: mathematics meets green industry", project code: 202248TY47, CUP: E53D23005430006, and support under the National Recovery and Resilience Plan (NRRP) funded by the European Union - NextGenerationEU - Project Title "Mathematical Modeling of Biodiversity in the Mediterranean sea: from bacteria to predators, from meadows to currents", project code: P202254HT8, CUP: E53D23017900001.

This paper has been performed under the auspices of the G.N.F.M. of I.N.d.A.M.

Conflict of interest

The authors declare no conflicts of interest.

References

1. F. Abbas, R. Sudarsan, H. J. Eberl, Longtime behavior of one-dimensional biofilm models with shear dependent detachment rates, *Math. Biosci. Eng.*, **9** (2012), 215–239. https://doi.org/10.3934/mbe.2012.9.215
2. D. Aregba-Driollet, F. Diele, R. Natalini, A mathematical model for the sulphur dioxide aggression to calcium carbonate stones: numerical approximation and asymptotic analysis, *SIAM J. Appl. Math.*, **64** (2004), 1636–1667. https://doi.org/10.1137/S003613990342829X
3. A. Augustyniak, P. Sikora, B. Grygorcewicz, D. Despot, B. Braun, R. Rakoczy, et al., Biofilms in the gravity sewer interfaces: making a friend from a foe, *Rev. Environ. Sci. Biotechnol.*, **20** (2021), 795–813. https://doi.org/10.1007/s11157-021-09582-0
4. A. Baldanza, V. Loianno, G. Mensitieri, G. Scherillo, Predictive approach for the solubility and permeability of binary gas mixtures in glassy polymers based on an NETGP-NRHB model, *Ind. Eng. Chem. Res.*, **61** (2022), 3439–3456. https://doi.org/10.1021/acs.iecr.1c04864
5. M. Berlanga, R. Guerrero, Living together in biofilms: the microbial cell factory and its biotechnological implications, *Microb. Cell Fact.*, **15** (2016), 165. https://doi.org/10.1186/s12934-016-0569-5

6. M. Böhm, J. Devinny, F. Jahani, G. Rosen, On a moving-boundary system modeling corrosion in sewer pipes, *Appl. Math. Comput.*, **92** (1998), 247–269. https://doi.org/10.1016/S0096-3003(97)10039-X

7. M. Böhm, J. Devinny, F. Jahani, F. B. Mansfeld, I. G. Rosen, C. Wang, A moving boundary diffusion model for the corrosion of concrete wastewater systems: simulation and experimental validation, *Proceedings of the 1999 American Control Conference (Cat. No. 99CH36251)*, **3** (1999), 1739–1743. https://doi.org/10.1109/ACC.1999.786137

8. G. Bretti, M. Ceseri, R. Natalini, A moving boundary problem for reaction and diffusion processes in concrete: carbonation advancement and carbonation shrinkage, *Discret. Contin. Dyn. Syst.-S*, **15** (2022), 2033–2052. https://doi.org/10.3934/dcdss.2022092

9. M. F. Carfora, I. Torcicollo, A fractional-in-time prey–predator model with hunting cooperation: qualitative analysis, stability and numerical approximations, *Axioms*, **10** (2021), 78. https://doi.org/10.3390/axioms10020078

10. F. Clarelli, A. Fasano, R. Natalini, Mathematics and monument conservation: free boundary models of marble sulfation, *SIAM J. Appl. Math.*, **69** (2008), 149–168. https://doi.org/10.1137/070695125

11. H. Eberl, E. Morgenroth, D. Noguera, C. Picioreanu, B. Rittmann, M. van Loosdrecht, et al., *Mathematical modeling of biofilms*, Vol. 5, IWA Publishing, 2006. https://doi.org/10.2166/9781780402482

12. S. V. Fedosov, S. A. Loginova, Mathematical model of concrete biological corrosion, *Mag. Civ. Eng.*, **99** (2020), 9906. https://doi.org/10.18720/MCE.99.6

13. H. Flemming, T. R. Neu, D. J. Wozniak, The EPS matrix: the "house of biofilm cells", *J. Bacteriol.*, **189** (2007), 7945–7947. https://doi.org/10.1128/jb.00858-07

14. H. C. Flemming, EPS–Then and now, *Microorganisms*, **4** (2016), 41. https://doi.org/10.3390/microorganisms4040041

15. L. Frunzo, V. Luongo, M. R. Mattei, A. Tenore, Qualitative analysis and simulations of the biological fouling problem on filtration membranes, *Partial Differ. Equ. Appl. Math.*, **8** (2023), 100557. https://doi.org/10.1016/j.padiff.2023.100557

16. R. M. Furzeland, A comparative study of numerical methods for moving boundary problems, *IMA J. Appl. Math.*, **26** (1980), 411–429. https://doi.org/10.1093/imamat/26.4.411

17. M. Hong, D. Niu, Q. Fu, Z. Hui, Z. Wan, Insights into bio-deterioration of concrete exposed to sewer environment: a case study, *Constr. Build. Mater.*, **412** (2024), 134835. https://doi.org/10.1016/j.conbuildmat.2023.134835

18. H. S. Jensen, A. H. Nielsen, T. Hvitved-Jacobsen, J. Vollertsen, Modeling of hydrogen sulfide oxidation in concrete corrosion products from sewer pipes, *Water Environ. Res.*, **81** (2009), 365–373. https://doi.org/10.2175/106143008X357110

19. H. S. Jensen, P. N. Lens, J. L. Nielsen, K. Bester, A. H. Nielsen, T. Hvitved-Jacobsen, et al., Growth kinetics of hydrogen sulfide oxidizing bacteria in corroded concrete from sewers, *J. Hazard. Mater.*, **189** (2011), 685–691. https://doi.org/10.1016/j.jhazmat.2011.03.005

20. I. Klapper, J. Dockery, Mathematical description of microbial biofilms, *SIAM Rev.*, **52** (2010), 221–265. https://doi.org/10.1137/080739720

21. J. Knisz, R. Eckert, L. M. Gieg, A. Koerdt, J. S. Lee, E. R. Silva, et al., Microbiologically influenced corrosion–more than just microorganisms, *FEMS Microbiol. Rev.*, **47** (2023), 1–33. https://doi.org/10.1093/femsre/fuad041

22. L. Kong, M. Han, X. Yang, Evaluation on relationship between accelerated carbonation and deterioration of concrete subjected to a high-concentrated sewage environment, *Constr. Build. Mater.*, **237** (2020), 117650. https://doi.org/10.1016/j.conbuildmat.2019.117650

23. X. Li, L. O'Moore, Y. Song, P. L. Bond, Z. Yuan, S. Wilkie, et al., The rapid chemically induced corrosion of concrete sewers at high H_2S concentration, *Water Res.*, **162** (2019), 95–104. https://doi.org/10.1016/j.watres.2019.06.062

24. W. Li, T. Zheng, Y. Ma, J. Liu, Current status and future prospects of sewer biofilms: their structure, influencing factors, and substance transformations, *Sci. Total Environ.*, **695** (2019), 133815. https://doi.org/10.1016/j.scitotenv.2019.133815

25. X. Liu, D. Niu, X. Li, Y. Lv, Effects of $Ca(OH)_2$–$CaCO_3$ concentration distribution on the pH and pore structure in natural carbonated cover concrete: a case study, *Constr. Build. Mater.*, **186** (2018), 1276–1285. https://doi.org/10.1016/j.conbuildmat.2018.08.041

26. V. Loianno, G. Mensitieri, A novel dynamic method for the storage of calibration gas mixtures based on thermal mass flow controllers, *Meas. Sci. Technol.*, **33** (2022), 065017. https://doi.org/10.1088/1361-6501/ac5a2f

27. R. A. Luimes, F. A. M. Rooyackers, A. S. J. Suiker, F. H. L. R. Clemens, E. Bosco, A novel approach for the lifetime prediction and structural health monitoring of concrete sewer systems exposed to biogenic sulphide corrosion, *Cement Concrete Res.*, **181** (2024), 107517. https://doi.org/10.1016/j.cemconres.2024.107517

28. M. Mora, L. R. López, J. Lafuente, J. Pérez, R. Kleerebezem, M. C. M. van Loosdrecht, et al., Respirometric characterization of aerobic sulfide, thiosulfate and elemental sulfur oxidation by S-oxidizing biomass, *Water Res.*, **89** (2016), 282–292. https://doi.org/10.1016/j.watres.2015.11.061

29. T. Mori, M. Koga, Y. Hikosaka, T. Nonaka, F. Mishina, Y. Sakai, et al., Microbial corrosion of concrete sewer pipes, H_2S production from sediments and determination of corrosion rate, *Water Sci. Technol.*, **23** (1991), 1275–1282. https://doi.org/10.2166/wst.1991.0579

30. T. Mori, T. Nonaka, K. Tazaki, M. Koga, Y. Hikosaka, S. Noda, Interactions of nutrients, moisture and pH on microbial corrosion of concrete sewer pipes, *Water Res.*, **26** (1992), 29–37. https://doi.org/10.1016/0043-1354(92)90107-F

31. C. V. Nikolopoulos, Macroscopic models for a mushy region in concrete corrosion, *J. Eng. Math.*, **91** (2015), 143–163. https://doi.org/10.1007/s10665-014-9743-0

32. S. Okabe, M. Odagiri, T. Ito, H. Satoh, Succession of sulfur-oxidizing bacteria in the microbial community on corroding concrete in sewer systems, *Appl. Environ. Microbiol.*, **73** (2007), 971–980. https://doi.org/10.1128/AEM.02054-06

33. W. Olmstead, H. Hamlin, Converting portions of the Los Angeles outfall sewer into a septic tank, *Eng. News*, **44** (1900), 317–318.

34. C. D. Parker, The corrosion of concrete, 1. The isolation of a species of bacterium associated with the corrosion of concrete exposed to atmospheres containing hydrogen sulphide, *Aust. J. Exp. Biol. Med. Sci.*, **23** (1945), 81–90. https://doi.org/10.1038/icb.1945.13

35. C. Picioreanu, M. C. Van Loosdrecht, J. J. Heijnen, Two-dimensional model of biofilm detachment caused by internal stress from liquid flow, *Biotech. Bioeng.*, **72** (2001), 205–218.

36. L. Pokorna-Krayzelova, D. Vejmelková, L. Selan, P. Jenicek, E. I. Volcke, J. Bartacek, Final products and kinetics of biochemical and chemical sulfide oxidation under microaerobic conditions, *Water Sci. Technol.*, **78** (2018), 1916–1924. https://doi.org/10.2166/wst.2018.485

37. S. K. Pramanik, M. Bhuiyan, D. Robert, R. Roychand, L. Gao, I. Cole, et al., Bio-corrosion in concrete sewer systems: mechanisms and mitigation strategies, *Sci. Total Environ.*, **921** (2024), 171231. https://doi.org/10.1016/j.scitotenv.2024.171231

38. D. J. Roberts, D. Nica, G. Zuo, J. L. Davis, Quantifying microbially induced deterioration of concrete: initial studie, *Int. Biodeter. Biodegr.*, **49** (2002), 227–234. https://doi.org/10.1016/S0964-8305(02)00049-5

39. F. A. M. Rooyackers, E. Bosco, A. S. J. Suiker, F. H. L. R. Clemens, A chemo-mechanical model for biogenic sulphide corrosion of concrete, *Cement Concrete Res.*, **160** (2022), 106809. https://doi.org/10.1016/j.cemconres.2022.106809

40. F. Russo, M. R. Mattei, A. Tenore, B. D'Acunto, V. Luongo, L. Frunzo, Analysis and simulations of a free boundary problem modelling phototrophic granular biofilms, *Discret. Contin. Dyn. Syst.-B*, **29** (2024), 4946–4972. https://doi.org/10.3934/dcdsb.2024073

41. A. Safari, Z. Tukovic, M. Walter, E. Casey, A. Ivankovic, Mechanical properties of a mature biofilm from a wastewater system: from microscale to macroscale level, *Biofouling*, **31** (2015), 651–664. https://doi.org/10.1080/08927014.2015.1075981

42. E. Samson, J. Marchand, K. A. Snyder, Calculation of ionic diffusion coefficients on the basis of migration test results, *Mat. Struct.*, **36** (2003), 156–165. https://doi.org/10.1007/BF02479554

43. A. K. Singh, *Microbially induced corrosion and its mitigation*, Springer, 2020. https://doi.org/10.1007/978-981-15-8019-2

44. Y. Song, Y. Tian, X. Li, J. Wei, H. Zhang, P. L. Bond, et al., Distinct microbially induced concrete corrosion at the tidal region of reinforced concrete sewers, *Water Res.*, **150** (2019), 392–402. https://doi.org/10.1016/j.watres.2018.11.083

45. P. S. Stewart, A model of biofilm detachment, *Biotech. Bioeng.*, **41** (1993), 111–117. https://doi.org/10.1002/bit.260410115

46. P. S. Stewart, Diffusion in biofilms, *J. Bacteriol.*, **185** (2003), 1485–1491. https://doi.org/10.1128/jb.185.5.1485-1491.2003

47. A. Tenore, F. Russo, J. Jacob, J. D. Grattepanche, B. Buttaro, I. Klapper, A mathematical model of diel activity and long time survival in phototrophic mixed-species subaerial biofilms, *Bull. Math. Biol.*, **86** (2024), 123. https://doi.org/10.1007/s11538-024-01348-3

48. J. Vincent, A. Tenore, M. R. Mattei, L. Frunzo, Modelling drinking water biofilms: bacterial adhesion and *Legionella pneumophila* necrotrophic growth, *Commun. Nonlinear Sci. Numer. Simul.*, **128** (2024), 107639. https://doi.org/10.1016/j.cnsns.2023.107639

49. J. Vollertsen, A. H. Nielsen, H. S. Jensen, T. Wium-Andersen, T. Hvitved-Jacobsen, Corrosion of concrete sewers–The kinetics of hydrogen sulfide oxidation, *Sci. Total Environ.*, **394** (2008), 162–170. https://doi.org/10.1016/j.scitotenv.2008.01.028

50. S. Wang, H. Zhu, G. Zheng, F. Dong, C. Liu, Dynamic changes in biofilm structures under dynamic flow conditions, *Appl. Environ. Microbiol.*, **88** (2022), e01072-22. https://doi.org/10.1128/aem.01072-22

51. O. Wanner, W. Gujer, A multispecies biofilm model, *Biotech. Bioeng.*, **28** (1986), 314–328. https://doi.org/10.1002/bit.260280304

52. S. Wei, Z. Jiang, H. Liu, D. Zhou, M. Sanchez-Silva, Microbiologically induced deterioration of concrete: a review, *Braz. J. Microbiol.*, **44** (2013), 1001–1007. https://doi.org/10.1590/S1517-83822014005000006

53. M. Wu, T. Wang, K. Wu, L. Kan, Microbiologically induced corrosion of concrete in sewer structures: a review of the mechanisms and phenomena, *Constr. Build. Mater.*, **239** (2020), 117813. https://doi.org/10.1016/j.conbuildmat.2019.117813

54. H. Yuan, P. Dangla, H. Chen, P. Chatellier, T. Chaussadent, Modelling of H2S attack of concrete in sewer pipes, *The Fourth RILEM International Symposium on Concrete Modelling (CONMOD 2014)*, 2014, 425–431.

55. H. Yuan, P. Dangla, H. Chen, P. Chatellier, T. Chaussadent, Degradation modeling of concrete submitted to biogenic acid attack, *Cement Concrete Res.*, **70** (2015), 29–38. https://doi.org/10.1016/j.cemconres.2015.01.002

56. L. Zhang, P. De Schryver, B. De Gusseme, W. De Muynck, N. Boon, W. Verstraete, Chemical and biological technologies for hydrogen sulfide emission control in sewer systems: a review, *Water Res.*, **42** (2008), 1–12. https://doi.org/10.1016/j.watres.2007.07.013

AIMS Press